Available online at www.sciencedirect.com
ScienceDirect
Journal of the European Ceramic Society 30 (2010) 1775–1783
www.elsevier.com/locate/jeurceramsoc

Steel particles–porcelain stoneware composite tiles: An advanced experimental–computational approach

V. Cannillo [a], L. Esposito [b], G. Pellicelli [c], A. Sola [a,*], A. Tucci [b]

[a] *Dipartimento di Ingegneria dei Materiali e dell'Ambiente, Università di Modena e Reggio Emilia, Via Vignolese 905, 41100 Modena, Italy*
[b] *Centro Ceramico Bologna, Via Martelli 26, 40138 Bologna, Italy*
[c] *Granitifiandre S.p.A., Via Radici Nord 112, 42014 Casalgrande (RE), Italy*

Received 12 November 2009; received in revised form 11 December 2009; accepted 20 January 2010
Available online 1 March 2010

Abstract

Innovative porcelain stoneware tiles with a surface layer containing 2.4 wt% of stainless-steel particles were produced by the Double Charge Technology. Considering this layer as a composite material, the effects of the metal particles on the mechanical behaviour of the ceramic matrix were extensively investigated in terms of Young's modulus, fracture toughness and flexural strength. With this aim, composite materials were prepared by using the same silicate-based ceramic matrix with increasing weight percentages of the same stainless-steel powder. The composites were accurately characterised. In particular, due to the high sintering temperature, possible changes at the interface between metal particles and ceramic matrix were thoroughly analysed by means of SEM and EDS microanalysis. To clarify the role of the observed chromium-rich interphase on the mechanical behaviour of the steel particles–stoneware composites, analytical equations were used and simulations were performed by using the Object Oriented Finite (OOF) element method.

Keywords: Composites; Mechanical properties; Porcelain stoneware; Metal; Finite element simulations

1. Introduction

In spite of their relevant properties (high elastic modulus and superficial hardness; good wear resistance; superior thermal stability; generally good chemical resistance), the use of ceramic materials in structural applications is limited by their brittleness. In order to improve the fracture toughness of ceramic materials, a ductile phase could be introduced. This approach has been widely investigated in the literature, with a particular focus on advanced ceramics, such as alumina,[1] reinforced with fibres and metal particles, both uniformly distributed[2] and spatially graded[3] in the ceramic matrix.

Recently, with the aim to confer a new aesthetic effect to porcelain stoneware tiles, the addition of metal particles into a porcelain stoneware tile was proposed. The resulting product, which can be described as a metal–stoneware composite, after the polishing of its working surface, was characterised by mirror-like dots, i.e. the steel particles, embedded in the ceramic matrix. The aesthetic effect was intensified by the introduction of $CoAl_2O_4$ in the ceramic matrix, which assumes a deep blue colour. However it is likely that the metal particles addition could have modified not only the appearance, but also the mechanical behaviour of the original ceramic matrix.

The aim of this work is therefore a wide-range investigation of the mechanical behaviour of such composite systems, including both the elastic properties and the fracture mechanics. Another original contribution is given by the analysis of the interface that developed between the metal particles and the ceramic matrix during the sintering process. Both analytical equations and microstructure-based finite element simulations were applied to investigate the role of the interface on the elastic response of the composites and the propagation of cracks. Indeed, refined modelling tools, derived from the field of advanced materials engineering, were required to achieve a deeper insight into the mechanical properties of the steel particle–stoneware composites.

* Corresponding author. Tel.: +39 059 2056281; fax: +39 059 2056243.
E-mail address: antonella.sola@unimore.it (A. Sola).

0955-2219/$ – see front matter © 2010 Elsevier Ltd. All rights reserved.
doi:10.1016/j.jeurceramsoc.2010.01.041

Table 1
Mineralogical composition of the ceramic matrix.

Phase	wt%
Quartz	11.1 ± 0.1
Mullite	1.5 ± 0.6
Plagioclase	1.2 ± 0.3
$CoAl_2O_4$	3.3 ± 0.2
Glass	82.9 ± 1.4

Table 3
Main properties of the constituent phases.[4,6].

	Stainless-steel particles	Silicate-based ceramic matrix
E (GPa)	193.0	68.7
ν	0.3	0.3
α (K^{-1})	18×10^{-6}	7×10^{-6}
K_{IC} (MPa $m^{1/2}$)	100.0	1.4

2. Materials and methods

In the present research, a commercially available product was considered,[4] constituted by a ceramic body and a composite surface layer, produced by using the double charge technology (DCT). In its turn, the composite surface layer had stainless-steel spherical particles embedded in the silicate-based ceramic matrix.

Since the most innovative feature of the tiles was the presence of the metal particles, the research was specifically addressed to the composite surface layer. As already mentioned, the matrix was a silicate-based ceramic system, whose mineralogical composition was determined by means of X-ray diffraction analysis. The data collection was performed by using a PW1710, Philips, instrument, operated in the angular range 10–80° 2θ with steps of 0.02° and 5 s/step. The Rietveld refinement was performed using GSAS.[5] The results are reported in Table 1.

The metal particles were stainless-steel AISI 316L spheres, whose average size lied in the 250–600 μm range. Four different systems, characterised by increasing amounts of metal particles and labelled Mixes 1–4, were analysed and computationally modelled. The weight and volume fractions of the steel particles in the four composite systems are listed in Table 2. The weight fractions are reported because they are of technological interest; the volume fractions are important because they are commonly used in analytical and computational approaches.

It should be underlined that, in the present context, the ceramic matrix was assumed to be uniform, since local heterogeneities were disregarded and mean properties were considered. Table 3 summarises the elastic modulus (E), Poisson's coefficient (ν), coefficient of thermal expansion (α) and fracture toughness (K_{IC}) of the constituent phases, as determined by the experimental tests or deduced from the literature.[4,6] In particular, as regards the ceramic matrix, some tiles were manufactured using the ceramic body alone, without adding the metal particles. These samples were characterised (SEM, EDS, XRD, micro-indentation, three- and four-point bending tests) in order to define the properties of the ceramic matrix alone.[4] Since it was not possible to test the metal particles directly, for the AISI 316L stainless-steel phase typical mechanical data were taken from the literature.[6]

Table 2
Weight percent, W_p, and volume percent, V_p, of the stainless-steel particles present in the four tested Mixes.

	W_p (%)	V_p (%)
Mix 1	2.4	0.7
Mix 2	4.8	1.5
Mix 3	7.2	2.3
Mix 4	32.0	12.3

Previous studies demonstrated the relevance of the residual porosity on the mechanical behaviour of ceramic tiles.[7] For this reason, the mean porosity of the pure ceramic tiles and that of the four Mixes containing the metal particles were evaluated by means of SEM image analysis (ImageTool). For each sample 10 images (50× back scattered micrographs) of mirror-like polished samples were considered in order to have statistical data.

2.1. Analytical approach

The analytical equations were applied assuming that the four Mixes are describable as bi-phasic composites (ceramic matrix + metal particles in various amounts).

A first evaluation of the elastic properties of the four Mixes can be based on analytical equations frequently used for composite materials, such as the Voigt model, the Reuss model and the Hashin and Shtrikman bounds.[8]

The Voigt and the Reuss models are averaging schemes that originally apply to long fibre composites and assume the constituents to be in parallel arrangement. According to the Voigt model, the constituents of the composite system experience an isostrain loading condition; vice versa, according to the Reuss model, the constituents are subjected to an isostress. Accordingly, the effective modulus of a two-phase composite is given by the relation (1):

$$E_V = E_1 V_1 + E_2(1 - V_1) \quad (1)$$

for the Voigt model[8] and by the relation (2):

$$E_R = \frac{1}{(V_1/E_1) + ((1 - V_1)/E_2)} \quad (2)$$

for the Reuss model.[8] In both cases, V_1 is the volume fraction of the phase 1; E_1 and E_2 are the elastic modules of the phase 1 and phase 2, respectively.

The Hashin and Shtrikman bounds were derived for macroscopically isotropic and quasi-homogeneous composites, characterised by a uniform distribution of the reinforcing particles into the matrix. Eq. (3) gives the upper and lower bounds of the bulk (K) and shear (G) modules of the composite[8]:

$$K_c^u = K_p + \frac{1 - V_p}{(1/(K_m - K_p)) + (3V_p/(3K_p + 4G_p))}$$
$$K_c^l = K_m + \frac{V_p}{(1/(K_p - K_m)) + (3(1 - V_p)/(3K_m + 4G_m))}$$
$$G_c^u = G_p + \frac{1 - V_p}{(1/(G_m - G_p)) + (6V_p(K_p - 2G_p)/(5G_p(3K_p + 4G_p)))}$$
$$G_c^l = G_m + \frac{V_p}{(1/(G_p - G_m)) + (6(1 - V_p)(K_m - 2G_m)/(5G_m(3K_m + 4G_m)))} \quad (3)$$

where V_p is the particle volume fraction; K_p, K_m and K_c are the bulk modules of the particles, the matrix and the composite material; G_p, G_m and G_c are the corresponding shear modules. The superscripts u and l identify the upper and lower bounds.

The upper and lower bounds for the elastic modulus of the composite can be calculated respectively from the upper and lower values of K_c and G_c using Eq. (4)[8]:

$$E_{HS} = \frac{9K_cG_c}{3K_c + G_c} \quad (4)$$

The bulk and shear modules of the constituent phases were calculated from the values of the elastic modulus (E) and the Poisson's coefficient (ν) reported in Table 3, assuming an isotropic behaviour of the metal particles and the ceramic matrix and using the relations (5):

$$K = \frac{E}{3(1 - 2\nu)}$$
$$G = \frac{E}{2(1 + \nu)} \quad (5)$$

2.2. Computational model

The computational simulations were performed by using OOF, the Object Oriented Finite element method, a software developed by N.I.S.T. and M.I.T. (U.S.A.) that is able to apply the finite element method at the microscale, using microstructural images and constituent phase properties as input data.[9,10]

Due to its flexibility and reliable modelling of the actual microstructure of materials, OOF has been applied to simulate a variety of systems, including very complicated ones, such as multiphase and functionally graded composites.[7,11–29]

Representative microstructures for the four Mixes were created by using a specific code, developed ad hoc, which made it possible to set the minimum and maximum size of the particles as well as the volume fraction of the constituent phases. As already mentioned, according to the metallographic characterization, the particle size varied between 250 μm and 600 μm[4]; the volume fractions were fixed according to Table 2. A typical microstructural image associated with Mix 1 is shown in Fig. 1a. In order to have statistical data, five representative microstructures were considered for each Mix. They are all reported in Fig. 2. These images can be considered "representative" of the real microstructure of the four Mixes because they include the same volume fraction of steel particles as the corresponding Mix, the sizes of the particles reproduce the experimental data (they are in the 250–600 μm range) and the particles are randomly distributed as experimentally observed in the samples.

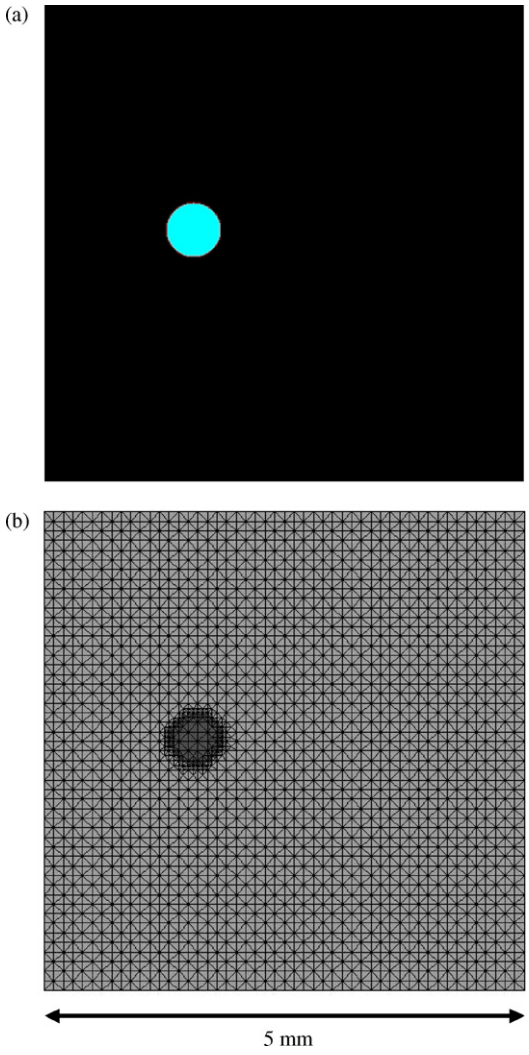

Fig. 1. Representative microstructure for Mix 1 (a) and corresponding finite element mesh (b).

Each microstructural image was mapped onto a finite element mesh; as an example, the grid corresponding to the microstructure in Fig. 1a is shown in Fig. 1b. If required, the mesh can be progressively refined, with a particular attention for the interface between the particles and the matrix, which is usually a critical point where local stresses are expected to concentrate.

The characteristic properties of the constituent phases were assigned according to Table 3. Then, the elastic properties of the four Mixes were determined by simulating tensile tests by means of OOF.[9,10] In the virtual tests, a small (0.1%) uniaxial strain was imposed. At first, "isotropic elements" (available in OOF) were used and a perfect bonding was assumed between the particles and the matrix. The assumption of a perfect bonding was preliminarily accepted because it also underlies the analytical equations.[8] However a more refined model was developed by modifying the representative microstructural images and introducing a weak interface, which was attributed a relatively low elastic modulus (0.01 GPa) and the same Poisson's coefficient and coefficient of thermal expansion as the ceramic matrix. All

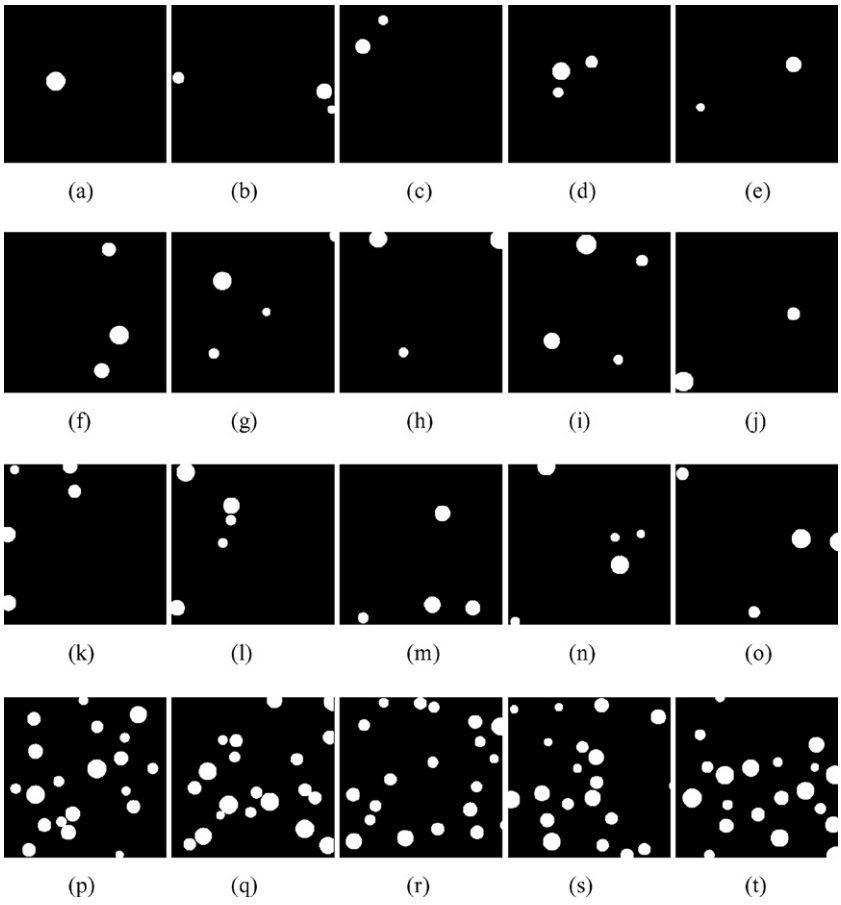

Fig. 2. Representative images for Mix 1 (a–e), Mix 2 (f–j), Mix 3 (k–o), and Mix 4 (p–t). For all images, model width = 5 mm.

the numerical results, obtained by the analytical equations and the computational simulations, were compared with the experimental data measured by means of 3-point bending tests.[4] In addition, OOF was used to develop specific models to predict the distribution of thermal residual stresses caused by the production process, in the final cooling down step from 600 °C to room temperature. Moreover, further attention was paid to the fracture mechanisms. With this aim, a different element type, i.e. the "Griffith element", was used instead of the "isotropic element". In fact the "Griffith element", which is available in OOF as well, was specifically implemented to simulate the crack propagation.

3. Results and discussion

The SEM image-based evaluation proved that the residual porosity in the pure ceramic tiles used to characterise the matrix and in the four Mixes was limited and independent on the presence and amount of metal particles, as it varied from 0.9 ± 0.2 for Mix 1 to 1.7 ± 0.3 for Mix 3. No evident flaws could be seen at the matrix–particle interface of the four Mixes. Since the residual porosity of the four Mixes was comparable, the observed difference in the mechanical behaviour of the four systems[4] was mainly caused by the presence of the metal particles and their interaction with the ceramic matrix. This suggests that the initial hypothesis of assuming the Mixes as bi-phasic systems (ceramic matrix + steel particles) could be reasonable. Moreover it is worth noting that the values reported in Table 3 were measured on ceramic tiles already containing residual pores. Hence, if the residual pores had been included as a third, independent phase in the analytical and computational models for the Mixes, they would have been accounted for twice; from this point of view, the properties reported in Table 3 for the ceramic matrix (implicitly) account also for the pores.

Since the metal particles are stiffer than the ceramic matrix, it would be reasonable to expect an improvement of the elastic properties of the composite by introducing the reinforcing phase; moreover, the elastic modulus should increase by increasing the particle volume fraction. In fact, as reported in Fig. 3, both the averaging schemes (Voigt and Reuss) and the Hashin and Shtrikman bounds predict that the elastic properties of the composites should be higher than those of the matrix and they should increase from Mix 1 to Mix 4.

Nevertheless, the experimental data clearly exhibit a quite opposite trend. As shown in Fig. 3, the experimental values are sensibly lower than the calculated ones and, even more strikingly, they get worse as the particle volume fraction increases.

The Voigt and Reuss schemes obviously offer a rough description of particle composites, since they were developed for oriented fibre composites,[8] however the Hashin and Shtrikman bounds usually give a good estimate of the overall mechanical properties of two-phase components, even when the

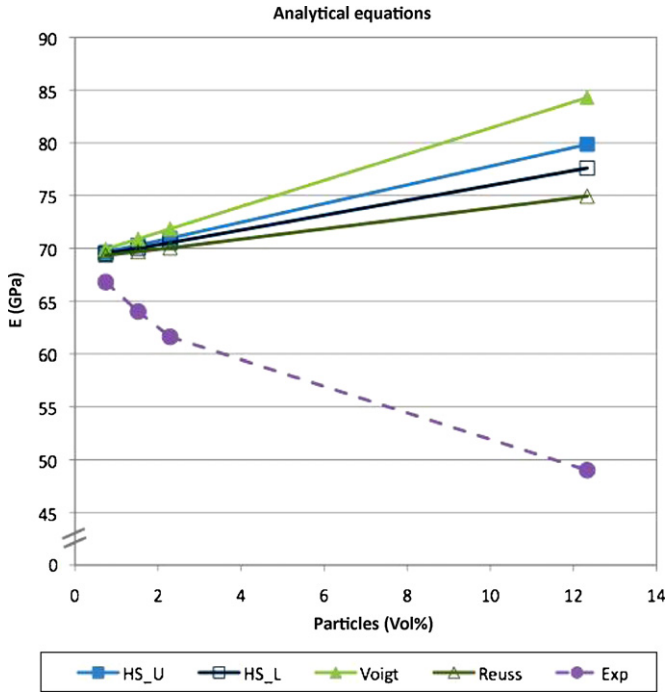

Fig. 3. Comparison between the results of the analytical equations and the experimental data: Hashin and Shtrikman upper bound, HS_U, light blue filled squares; Hashin and Shtrikman lower bound, HS_L, dark blue empty squares; Voight model, light green filled triangles; Reuss model, dark green empty triangles; experimental data, Exp, violet circles. (For interpretation of the references to colour in this figure legend, the reader is referred to the web version of the article.)

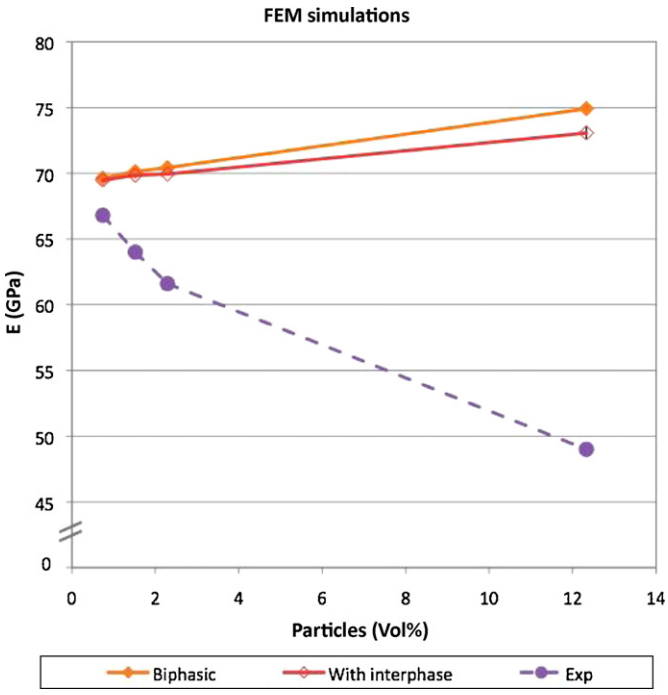

Fig. 4. Comparison between the results of the FEM simulations and the experimental data: simulations performed on the bi-phasic composites, orange filled markers; simulations performed introducing an interphase between the particles and the matrix, red empty markers; experimental data, violet circles. (For interpretation of the references to colour in this figure legend, the reader is referred to the web version of the article.)

characteristic modules of one phase are quite large as compared to those of the other phase, as in the present case.[30]

As shown in Fig. 4, the computational simulations performed by using OOF attained better results than the analytical equations, since the discrepancy with the experimental data is smaller. This is due to a more accurate modelling of the microstructure, since the microstructure-based FEM simulations account for several features, such as the real spatial position and particle size distribution of the metal particles, which are usually disregarded by analytical equations.[10] Nevertheless the gap between the computational output and the measured values is still sensible, especially for the Mix 4, which contains the highest particle volume fraction.

In order to justify the unusual mechanical behaviour of the composites under investigation, a more refined model should be set up. In particular, it is likely that the thermal process performed to sinter the composites could have promoted the development of a weak interphase between the metal particles and the surrounding ceramic phase. It is widely accepted that the presence of an interphase could significantly influence the behaviour of composite materials, especially if the reinforcing phase is nanosized and hence the interfacial area is extremely high.[28] In the present research the particles are relatively large, in the 250–600 μm range as previously mentioned, nevertheless the interfacial area is relevant especially in the systems containing a high volume fraction of particles, the same systems that deviate most strongly from the analytical and computational models. The hypothesis of the development of an interphase was confirmed by the SEM inspection of the composites. In fact, as already mentioned, no evident flaws could be seen at the interface, but a chromium-rich phase could be observed around all the metal particles, independently of their size and their volume fraction in the composite.[4] As an example, Fig. 5 shows the

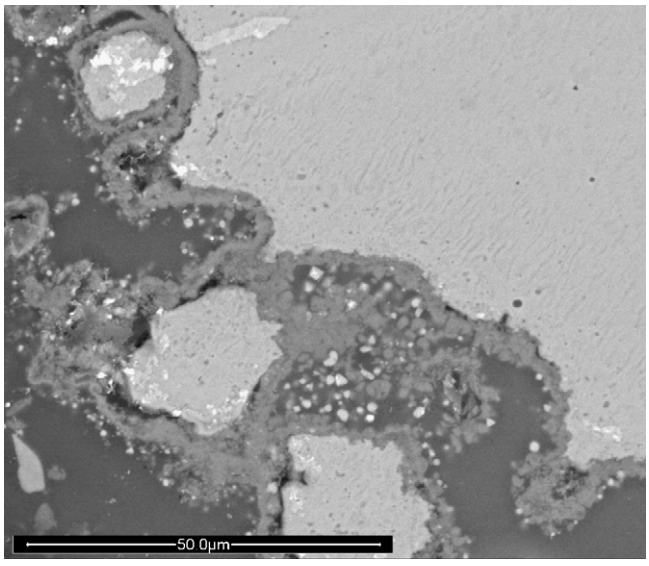

Fig. 5. SEM BE image of the polished cross section of Mix 1, showing the chromium-rich interphase developed between metal particles (light gray areas) and ceramic matrix (dark gray areas).

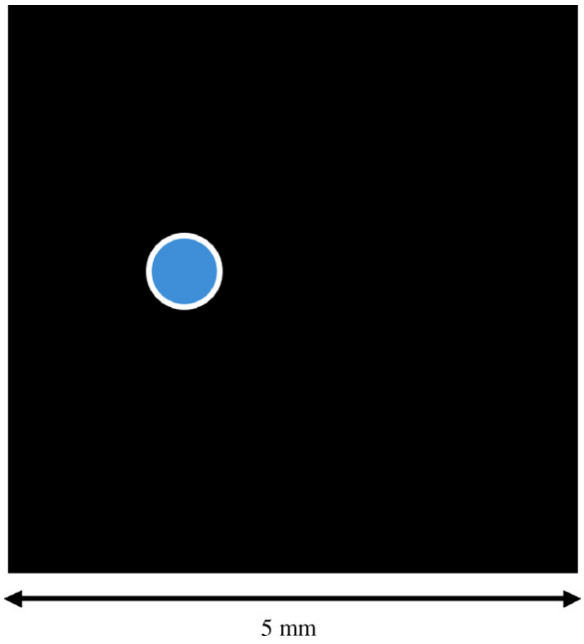

Fig. 6. Representative microstructure of the Mix 1 with the addition of the interphase. The image corresponds to the microstructure presented in Fig. 1a.

presence of the chromium-rich interphase around a particle in the Mix 1.

With the aim of accounting for this third phase, the computational model was properly modified. The same images used for the previous simulations were modified, introducing an interphase with an indicative (radial) thickness of 20 μm. Fig. 6 proposes the same representative microstructure of Fig. 1a with the addition of the interphase. Since the interphase is presumably weak, its elastic modulus was fixed to 0.01 GPa. The Poisson's coefficient and the coefficient of thermal expansion were assumed to be the same as those of the matrix (0.3 and 7 10^{-6} K^{-1}, respectively). As presented in Fig. 4, the presence of a weak interphase is expected to reduce the increment in the elastic properties of the Mixes, especially in those composites that contain a high volume fraction of particles. As previously mentioned, this is reasonable, since a high volume fraction of particles creates a very wide particle/matrix interface and therefore a significant volume fraction of the interphase.

In spite of the introduction of the weak interphase, as shown in Fig. 4 the modified model still overestimates the elastic properties of the composites. The lack of correspondence between the predicted values and the experimental ones is ascribable to a decay in the properties of the stainless-steel particles caused by the sintering heat treatment. In fact, the steel particles obviously experience a chromium depletion associated with the development of the observed chromium-rich interphase. Moreover it is well known that several stainless steels, if heated up to 500–800 °C, suffer an intergranular corrosion.[6] In fact it is thought that the heat treatment could promote a reaction between the carbon and the chromium of the stainless steel, inducing the creation of small particles of chromium carbide ($Cr_{23}C_6$) that preferentially precipitate at the grain boundaries. In the composite materials considered here, the migration of chromium from the steel particles to the interphase and the concomitant precipitation of chromium carbides at the grain boundaries are likely to affect the properties of the particles, reducing them with respect to the values listed in Table 3 and used in the simulations. In fact, as already mentioned, it was not possible to measure the mechanical properties on the metal particles directly and therefore data available in the literature were used for the AISI 316L stainless steel. This is reasonably the main reason for the overestimation of the mechanical properties of the four Mixes.

Further investigations were dedicated to the fracture toughness of the composite materials. Four-point bending tests proved that the fracture toughness moderately increased from 1.4 MPa $m^{1/2}$ for the ceramic matrix to 2.32 MPa $m^{1/2}$ for the Mix 3 and then decreased to 1.24 MPa $m^{1/2}$ for the Mix 4.[4] As recently reviewed by Yeomans, several toughening mechanisms can be active in ductile particle ceramic matrix composites, however the ideal situation is achieved when an advancing crack is attracted to a metal particle, then the particle debonds partially from the matrix and deforms plastically, thus absorbing energy and bridging the crack.[1] As regards the composite materials of the present research, the SEM inspection of the fractured samples, coupled with the analysis of indentation-induced cracks, proved that the steel particles actually attracted the advancing cracks, dissipating energy by various mechanisms such as crack blunting, crack deflection and even crack bridging via plastic deformation.[4] The effectiveness of the toughening mechanisms, however, appeared to be deeply influenced by the volume fraction of the metal particles. In principle, the toughness increment should increase with the volume fraction of the ductile particles; nevertheless, the performance of the Mix 4 was lower than that of the Mix 3. The decrease in the fracture toughness observed in the Mix 4 could be due to the weakening effect of the chromium-rich interphase, which prevailed on the strengthening mechanisms of the steel particles.

OOF was used to simulate the crack propagation in the composite systems. For the metal particles and the ceramic matrix, the values of the characteristic properties reported in Table 3 were considered. As already discussed for the simulation of the elastic properties, the available data for the metal phase should be used with great caution, since the firing process probably decreased them. For this reason, in a first approximation, the particles were assimilated to rigid inclusions, with a purely elastic behaviour. This hypothesis, which completely disregards the plastic deformation of the metal particles, is severe but precautionary, because it limits the overestimation of the toughening effect of the particles. As regards the interphase, its fracture toughness was assumed to be two orders of magnitude lower than that of the matrix. The crack propagation, simulated by applying the Griffith criterion (thanks to a specific element type available in OOF), was evidently influenced by the presence of the metal particles, since several microcracks developed around the metal particles and propagated along meandering paths governed by the metal particle distribution. Fig. 7 offers an example of the crack propagation in the Mix 4; in the simulation, an increasing strain was applied, with increment steps of 0.1%.

One more concern to consider is the development of thermal residual stresses caused by the relevant difference in the

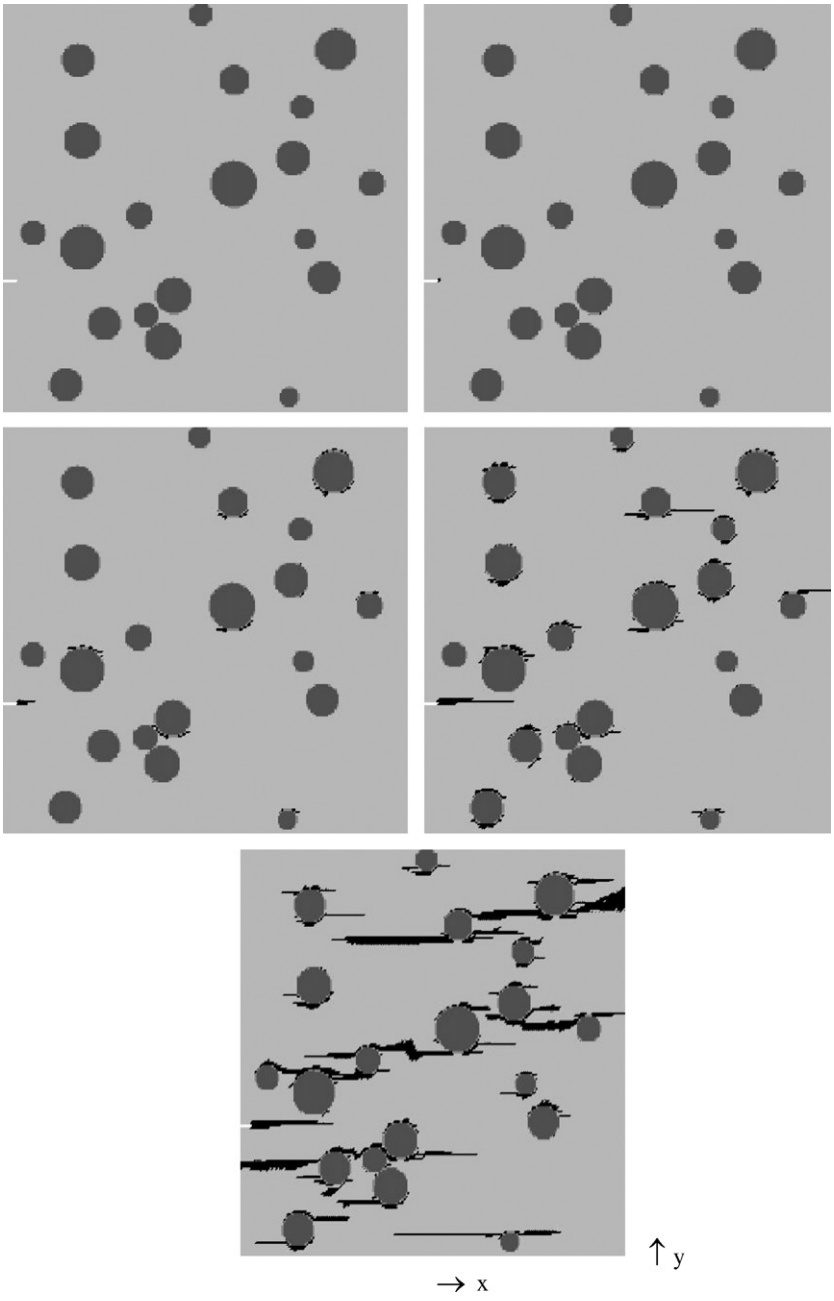

Fig. 7. Crack propagation in the Mix 4 for increasing applied strain in *y* direction. For all images: model width: 5 mm. In black: cracked elements.

coefficients of thermal expansion of the constituent phases. It is likely that, in presence of a sensible thermodilatometric mismatch, a high volume fraction of the metal particles may engender dangerous cracks able to by-pass the particles themselves.[1] With the aim of clarifying the entity of the thermal residual stresses in the composites, OOF was used to simulate the cooling down step at the end of the firing process, from 600 °C (when the system should not contain viscous phases any longer) to room temperature. The models also included the chromium-rich interphase, whose coefficient of thermal expansion was assumed to be the same as that of the matrix. Fig. 8 presents a direct comparison of the residual stresses in the Mix 1 and the Mix 4. The Mix 4 obviously experienced very high local stresses, whose peak values were mainly located around the metal particles. Moreover, in order to quantify the average stress state in the constituent phases, the mean hydrostatic stress σ_h was calculated according to Eq. (6):

$$\sigma_h = \frac{\sigma_I + \sigma_{II} + \sigma_{III}}{3} = \frac{Inv_1}{3} \quad (6)$$

where σ_I, σ_{II} and σ_{III} are the principal stresses and Inv_1 is the first invariant. The results for the simulations in Fig. 8 are shown in Table 4. It is evident that the average stress state in the constituent phases (tensile in the metal particles; compressive in the ceramic matrix) was more severe in the Mix 4, as a consequence of the higher interfacial area between the particles

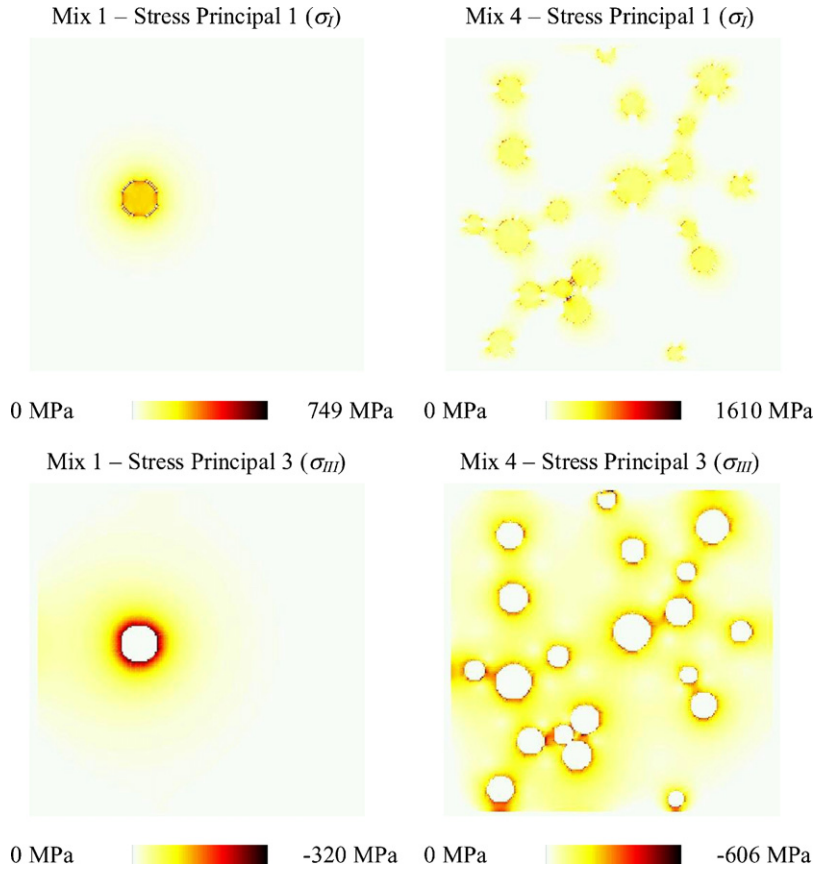

Fig. 8. Thermal residual stresses in the Mix 1 and Mix 4. The stress principal 1 is representative of a tensile stress state (positive values); the stress principal 3 is representative of a compressive stress state (negative value). For all images, model width = 5 mm.

Table 4
Mean hydrostatic stress (σ_h) in the constituent phases of the Mix 1 and the Mix 4. The values refer to the simulations in Fig. 8.

	σ_h (MPa)	
	Mix 1	Mix 4
Particles	191.3	485.6
Matrix	−1.9	−51.7

and the matrix. This result further justifies the lower fracture toughness achieved by the Mix 4 with respect to the other systems containing a lower amount of metal particles.

4. Conclusions

The introduction of stainless-steel particles into porcelain stoneware tiles was mainly motivated by aesthetic reasons, since the metal particles confer a bright sparkling appearance to the tile surface. However the introduction of metal particles into the ceramic matrix unavoidably affects its mechanical properties. According to the analytical schemes for two-phase composite systems, the metal particles are expected to increase the mechanical properties of the ceramic phase, but this prevision is disproved by the experimental evidence, since the measured elastic properties significantly decrease when the metal content increases. In order to justify this unusual behaviour, additional elements should be taken into account, in particular the formation of a weak chromium-rich interphase between the metal particles and ceramic matrix, the alteration of the characteristic properties of the stainless steel of the particles because of the sintering heat treatment and the development of not negligible thermal residual stresses.

References

1. Yeomans JA. Ductile particle ceramic matrix composites—Scientific curiosities or engineering materials? *Journal of the European Ceramic Society* 2008;**28**:1543–50.
2. Bartolomé JF, Beltrán JI, Gutiérrez-González CF, Pecharromán C, Muñoz MC, Moya JS. Influence of ceramic–metal interface adhesion on crack growth resistance of ZrO_2–Nb ceramic matrix composites. *Acta Materialia* 2008;**56**:3358–66.
3. Szafran M, Konopka K, Bobryk E, Kurzydłowski KJ. Ceramic matrix composites with gradient concentration of metal particles. *Journal of the European Ceramic Society* 2007;**27**:651–4.
4. Pellicelli G, Esposito L, Rambaldi E, Tucci A. Crack paths and toughening mechanisms in steel–porcelain stoneware ceramic matrix composites. *QUALIcer* 2008:85–94 [P. BC].
5. Larson AC, Von Dreele RB. *GSAS generan structure analysis system, LAUR 86-748*. USA: Los Alamos National Laboratory Report; 1994.
6. Callister Jr WD. *Materials science and engineering: an introduction*, 6th ed. Wiley, 2003.
7. Cannillo V, Esposito L, Rambaldi E, Sola A, Tucci A. Effect of porosity on the elastic properties of porcelainized stoneware tiles by a multi-layered model. *Ceramics International* 2009;**35**:205–11.

8. Wang M, Pan N. Elastic property of multiphase composites with random microstructures. *Journal of Computational Physics* 2009;**228**:5978–88.
9. Carter WC, Langer SA, Fuller Jr ER. *The OOF manual, version 1.0*; 1998.
10. Langer SA, Fuller Jr ER, Carter WC. OOF: an image-based finite element analysis of material microstructures. *Computing in Science and Engineering* 2001;**3**:15–23.
11. Saigal A, Fuller Jr ER, Langer SA, Carter WC, Zimmerman MH, Faber KT. Effect of interface properties on microcracking of iron titanate. *Scripta Materialia* 1998;**38**:1453–99.
12. Hsueh CH, Fuller Jr ER, Langer SA, Carter WC. Analytical and numerical analyses for two-dimensional stress transfer. *Materials Science and Engineering A* 1999;**268**:1–7.
13. Hsueh CH, Haynes JA, Lance MJ, Becher PF, Ferber MK, Fuller Jr ER, et al. Effects of interface roughness on residual stresses in thermal barrier coatings. *Journal of the American Ceramic Society* 1999;**82**:1073–5.
14. Zimmermann A, Fuller Jr ER, Rödel J. Residual stress distributions in ceramics. *Journal of the American Ceramic Society* 1999;**82**:3155–60.
15. Hsueh CH, Fuller Jr ER. Residual stresses in thermal barrier coating: effects of interface asperity curvature/height and oxide thickness. *Materials Science and Engineering A* 2000;**283**:46–55.
16. Cannillo V, Carter WC. Computation and simulation of reliability parameters and their variations in heterogeneous materials. *Acta Materialia* 2000;**48**:3593–605.
17. Zimmermann A, Carter WC, Fuller Jr ER. Damage evolution during microcracking of brittle solids. *Acta Materialia* 2001;**49**:127–37.
18. Zimmerman MH, Baskin DM, Faber KT, Fuller Jr ER, Allen AJ, Keane DT. Fracture of a textured anisotropic ceramic. *Acta Materialia* 2001;**49**:3231–42.
19. Vedula VR, Glass SJ, Saylor DM, Rohrer GS, Carter WC, Langer SA, et al. Residual-stress predictions in polycrystalline alumina. *Journal of the American Ceramic Society* 2001;**84**:2947–54.
20. Saigal A, Fuller Jr ER. Analysis of stresses in aluminium–silicon alloys. *Computational Materials Science* 2001;**21**:149–58.
21. Cannillo V, Corradi A, Leonelli C, Boccaccini AR. A simple approach for determining the in situ fracture toughness of ceramic platelets used in composite materials by numerical simulations. *Journal of Materials Science Letters* 2001;**20**:1889–91.
22. Cannillo V, Leonelli C, Boccaccini AR. Numerical models for thermal residual stresses in Al_2O_3 platelets/borosilicate glass matrix composites. *Materials Science and Engineering A* 2002;**323**:246–50.
23. Cannillo V, Leonelli C, Manfredini T, Montorsi M, Boccaccini AR. Computational simulations for the assessment of the mechanical properties of glass with controlled porosity. *Journal of Porous Materials* 2003;**10**: 189–200.
24. Cannillo V, Pellacani GC, Leonelli C, Boccaccini AR. Numerical modeling of the fracture behavior of a glass matrix composite reinforced with alumina platelets. *Composites Part A* 2003;**34**:43–51.
25. Wang Z, Kulkarni A, Deshpande S, Nakamura T, Herman H. Effects of pores and interfaces on effective properties of plasma sprayed zirconia coatings. *Acta Materialia* 2003;**51**:5319–34.
26. Cannillo V, Manfredini T, Montorsi M, Boccaccini AR. Investigation of the mechanical properties of Mo-reinforced glass–matrix composites. *Journal of Non-Crystalline Solids* 2004;**344**:88–93.
27. Cannillo V, Manfredini T, Montorsi M, Siligardi C, Sola A. Microstructure-based modelling and experimental investigation of crack propagation in glass-alumina functionally graded materials. *Journal of the European Ceramic Society* 2006;**26**:3067–73.
28. Cannillo V, Bondioli F, Lusvarghi L, Montorsi M, Avella M, Errico ME, et al. Modeling of ceramic particles filled polymer–matrix nanocomposites. *Composites Science and Technology* 2006;**66**:1030–7.
29. Dong Y, Bhattacharyya D, Hunter PJ. Experimental characterisation and object-oriented finite element modelling of polypropylene/organoclay nanocomposites. *Composites Science and Technology* 2008;**68**: 2864–75.
30. Cristescu ND, Cracium E-M, Soós E. *Mechanics of elastic composites*. Chapman & Hall/CRC, 2004.